Acoustic emission localization in composites using the signal power method and embedded transducers

Mario Emanuele De Simone[a], Stefano Cuomo[a], Francesco Ciampa[b], Michele Meo*[a], Sandro Nitschke[c], Andreas Hornig[c], Niels Modler[c]
[a]Dept. of Mechanical Engineering, University of Bath, Bath, BA2 7AY, UK
[b]Dept. of Mechanical Engineering Sciences, University of Surrey, Guildford, GU2 7XH, UK
[c]Technische Universität Dresden, Institute of Lightweight Engineering and Polymer Technology, Holbeinstraße 3, 01307 Dresden, Germany

*m.meo@bath.ac.uk;

ABSTRACT

This work proposes a novel technique for the localization of low-velocity impacts in composites without a-priori knowledge of the mechanical properties nor the speed of propagating waves, thus overcoming current limitations of existing impact localization methods. The proposed algorithm is based on the estimation of the power of acoustic emissions generated by impacts on a composite plate instrumented with embedded piezo-transducers. The signal power values calculated at sparse sensor locations are interpolated over the sample by using radial basis function networks. The impact coordinates on the specimen surface are estimated by a center-of-gravity method based on the interpolated power values. Experimental tests were performed by using both an instrumented impact hammer and a drop tower. The results obtained showed the validity of the presented approach, which was able to identify the impact locations with high level of accuracy.

Keywords: Impact localization, radial basis functions, signal power method, composite materials, embedded transducers

1. INTRODUCTION

Low-velocity impact localization in composite structures is currently a main concern for the aerospace engineering sector, as it is well known that such a class of materials are dramatically affected by out-of-plane impulsive loads. Indeed, despite their valuable in-plane mechanical properties, composite materials have low resistance towards low velocity impacts (LVI). Barely visible impact damage (BVID) caused by minimum energy impacts, could lead to a detriment of mechanical properties of the structures with possible catastrophic consequences. In this context, a technique capable to detect and localize impacts would make components and structures inspection faster with time savings in maintenance and operations. Several impact identification approaches have been proposed in literature. Early works are based on the triangulation technique [1] and are limited to isotropic structures, homogeneous materials and known wave speed. Ciampa and Meo [2] introduced a modified version of the triangulation technique in isotropic materials without prior knowledge of the wave speed. Kundu et al. [3, 4] proposed an algorithm based on the minimization of an error function, which was capable of locating the impact source in isotropic and anisotropic plate instrumented with four sensors. However, their algorithm required the knowledge of the direction dependence of the wave speed. Ciampa and Meo [5, 6] developed a technique, using six sensors, capable of localizing the impact location in anisotropic plate without prior knowledge of the mechanical properties nor the wave velocity, by solving a set of nonlinear equations using a combination of local and global optimization methods. De Simone and Ciampa [7] developed an impact localization method suitable for both isotropic and composite samples, which also required no prior knowledge of the wave speed propagating in the test samples. Their method relies on an optimal configuration of four piezo transducers, which allows linearization of well-known nonlinear system of equations for the estimation of the impact location. The Akaike information criterion (AIC) is used for the estimation of the time of arrival (TOA) of the elastic waves generated by the impact source.
Another approach able to identify the location of an impact event is the time reversal method, where impact localization is achieved by measuring the structural response on a set of calibration points on the specimen and cross-correlating these

recorded signals with the signal coming from an actual impact event [8-10]. The "impact cell" is estimated as the one with the maximum correlation coefficient, averaged among its corner points, and then the actual impact location is evaluated by a center-of-gravity method [11, 12].
This paper proposed a new impact localization algorithm based on the estimation of the signal power of measured elastic waves. The novelty of the proposed impact localization system is its intrinsic capability to pinpoint the impact location without the knowledge of the wave velocity, whilst minimising the number of receiver sensors using radial basis functions (RBF) networks. A sparse array of piezo-sensors embedded in a composite plate were used to record acoustic emissions caused by the impact event and to estimate the signal power values. The RBF approach was specifically employed to interpolate the power of acquired signals over the surface of the test sample. The impact location was finally estimated by a center-of-gravity method, involving all the power values and their spatial coordinates. As further remarks, this technique needs no material properties information, as well as wave speed dependency knowledge, neither a baseline calculated after a calibration process. It should be noted that the presented impact localization method is suitable when a high number of receiving sensors is present on the structure for monitoring the impact events.

2. SIGNAL POWER METHOD

As described in the Introduction section, the main goal of this research work id the localization of acoustic emissions sources in composite specimens when only the information of signals recorded after an impact event by a sparse array of *N* piezoelectric transducers is available. Furthermore, the piezo sensors are embedded inside the composite structure.
A signal power method was applied to overcome current limitations of existing impact localization methods, in a similar way to [13]. Indeed, when a structure has abundant sensors for monitoring impact events, the signal power due to impact loading can provide a good estimation for the impact location.
The proposed algorithm is divided in three parts: the first one (see Section 2.1) consists of calculating the power values related to the acquired signals in a given time window. In the second part (see Section 2.2), an interpolation process performed by using the radial basis function (RBF) approach is achieved in order to evaluate a power distribution over the entire considered sample. The third part (see Section 2.3) provides the localization of the impact event, which is achieved by the center-of-gravity method involving the interpolated power values and their corresponding spatial coordinates on the specimen surface.

2.1 Signal power calculation

If a generic time signal $s(t)$ is considered, it is well known that its energy, in a given time window, can be defined as:

$$E(t) = \int_{t_0}^{t_f} |s(t)|^2 \, dt \,, \tag{1}$$

where t_0 and t_f represent respectively the initial and final time of the considered time window.
The power of the same signal is defined as the mean of the energy value calculated by Eq. (1) over the time window length, identified as $t_f - t_0$:

$$P(t) = \frac{1}{t_f - t_0} \int_{t_0}^{t_f} |s(t)|^2 \, dt \,, \tag{2}$$

Once recorded the signals due to the impact event, Eq. (2) is applied in order to obtain *N* power values corresponding to the *N* piezo sensor locations. In this research work, only the first wave packet of the recorded signals was considered in the power calculation, as it is possible to eliminate signal ambiguities (e.g. the wave-reflections) considering a time window that includes only the first wave packets.

2.2 Radial basis function interpolation

After the calculation of power value at each sensor location in the test sample, Park et al. [13] obtained a smooth power distribution by interpolation, so that the interpolating surface satisfied the bi-harmonic equation and therefore had minimum curvature. In this work, signal power values were used as input of the radial basis function (RBF) approach. Particularly, power values associated to an arbitrary set of *M* points over the sample surface were obtained by the

knowledge of the *N* available power values, calculated as described in Section 2.1. The used RBF interpolation method is explained in detail in [14, 15].
In some recent works the authors demonstrated that hierarchical radial basis functions (RBFs) provide high accuracy in the data reconstruction when information related to a point on the structure is not available [11, 12]. In the proposed paper, the unknown data are the power values related to the *M* points on the sample surface, whose known spatial coordinates are the inputs of the RBF interpolation method, in addition to the known *N* power values to be interpolated and related to the sensor locations. The power value at each point on the sample was calculated by using the following augmented RBF interpolation considering a two-dimensional approach:

$$P(x_i, y_i) = \sum_{j=1}^{N} \lambda_j \, \phi\left(\sqrt{\left(x_i - x_j\right)^2 + \left(y_i - y_j\right)^2}\right) + \gamma_o + \gamma_1 x_i + \gamma_2 y_i \,, \quad 1 \le i \le M \,, \tag{3}$$

where x_i and y_i are coordinates of the i^{th} point of the arbitrary set of *M* points over the sample surface, x_j and y_j are coordinates of the j^{th} calibration point (where the power value necessary for the interpolation is known), λ_j and γ_k are the expansion coefficients and $\phi(\cdot)$ is a suitable radial basis function. The expansion coefficients were calculated as shown below, as solutions of a linear system of equations:

$$\begin{bmatrix} \lambda_1 \\ \vdots \\ \lambda_N \\ \gamma_1 \\ \gamma_2 \\ \gamma_o \end{bmatrix} = \begin{bmatrix} \phi_{1,1} & \dots & \phi_{1,N} & x_1 & y_1 & 1 \\ \vdots & \ddots & \vdots & \vdots & \vdots & \vdots \\ \phi_{N,1} & \dots & \phi_{N,N} & x_N & y_N & 1 \\ x_1 & \dots & x_N & 0 & 0 & 0 \\ y_1 & \dots & y_N & 0 & 0 & 0 \\ 1 & \dots & 1 & 0 & 0 & 0 \end{bmatrix}^{-1} \begin{bmatrix} P_1 \\ \vdots \\ P_N \\ 0 \\ 0 \\ 0 \end{bmatrix}, \tag{4}$$

where $P_1, \dots P_N$ are the power values at *N* transducer locations. As performed in other research works [11, 12] the thin plate spline (TPS), whose kernel is $\phi(\cdot) = (\cdot)^2 \, ln(\cdot)$, was used as radial basis function for its peculiar characteristics [16]. Once obtained the expansion coefficient values, they were substituted into Eq. (3) in order to calculate the power value at each point of the set *M*. The result of this process was the power distribution over the considered sample (see Figure 7).

2.3 Impact localization

Once estimated the signal power values, the location of the impact event was estimated by a center-of-gravity method [11, 12], involving the power values and the relative spatial coordinates [13]:

$$x_I = \frac{\sum_{i=1}^{M+N} x_i \, P_i}{\sum_{i=1}^{M+N} P_i}, \qquad y_I = \frac{\sum_{i=1}^{M+N} y_i \, P_i}{\sum_{i=1}^{M+N} P_i}, \tag{5}$$

where the calculation was performed considering the data from both the *N* calibration points and the arbitrary set of *M* points.

3. EXPERIMENTAL SET-UP

The investigated specimen panel, with dimensions 300 mm × 300 mm and cured thickness without piezo sensors equal to 1.52 mm, consists of 12 layers (0.11mm ply thickness) of Hexply 8552 UD prepreg material and one sensing layer (SL). The panel is manufactured within a vacuum press at 7 bar mould pressure and a two-step thermal curing cycle. The first ramp is from room temperature to 110°C, holding that temperature for one hour. The second ramp is to heat the panel to 180°C and holds it for two hours after cooling it back to room temperature. The lay-up sequence is as follows: $[0_2/90_2/0_2]_S$. The SL-layer is placed between play 10 and 11 and consists of two glass-fibre mats (each 30 g/m^2 and 0.1mm dry thickness) to isolate the 16 individual placed piezo ceramic elements. Each individual sensing element has a size of 10 mm × 10 mm and a thickness of 0.2 mm. Each sensing element is in enclosed within a double-sided polyamide carrier on which the electrode structure is screen-printed. Total thickness of the sensing element with polyamide carrier foils is 0.4 mm. Additionally two thin copper wires are connected on the screen-printed electrodes and peer out of the carrier foils at the other end to realize a soldered connection (see Figure 1a). To connect the sensing elements with the data acquisition system additional soldering terminals are placed at the outer corners of the panels, which are connected with the sensing elements

and are further isolated with polyimide adhesive tape (see Figure 1b and c). To ensure the easy accessibility to the soldering terminals after the manufacturing process the top pre-preg layers are cut out beforehand (see Figure 1d and e).

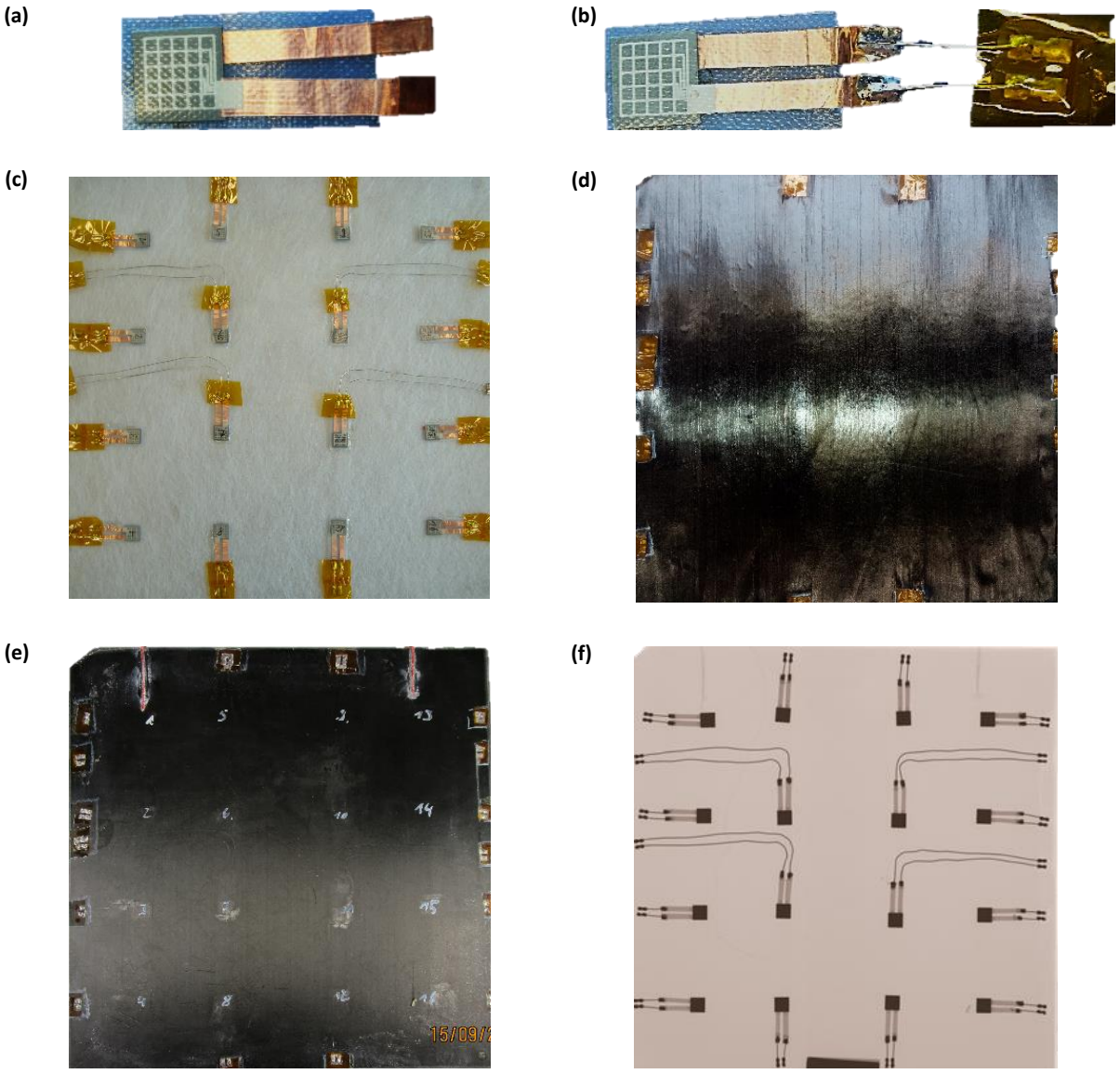

Figure 1. Steps of CFRP panel specimen manufacturing with integrated sensor elements: sensor preparation (a and b); sensor positioning and integration (c); pre-preg stacking (d); consolidated panel specimen (e); computed tomography scan (f).

The CFRP specimen considered for the experimental tests with the spatial coordinates of the used embedded transducers are shown in Figure 2:

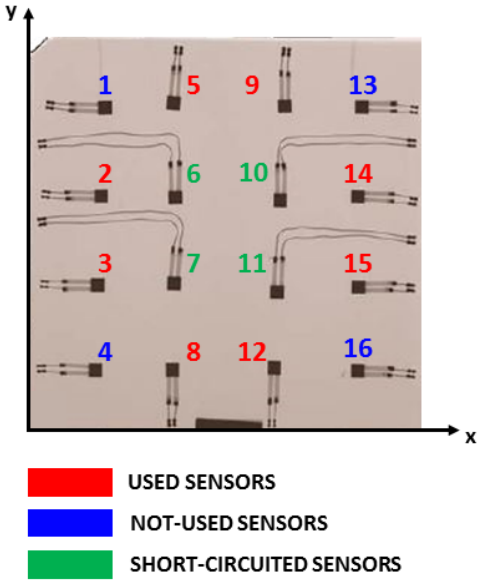

	x-Coordinate (mm)	y-Coordinate (mm)
SENSOR 2	53.7	176.8
SENSOR 3	51.9	109.6
SENSOR 5	107.8	246.1
SENSOR 8	108.7	46.8
SENSOR 9	190.5	244.9
SENSOR 12	185.1	49.2
SENSOR 14	246.7	179.2
SENSOR 15	248.2	111.4

Figure 2. CFRP specimen with embedded sensors and their spatial coordinates.

It should be noted that only eight sensors are used for the tests.
To validate the described algorithms, experimental impact tests were performed by using:

- a hand-held instrumented impact hammer (see Figure 3);
- a small free-drop tower (see Figure 4).

The signals were acquired with a sampling rate of 2 MHz.
Two different sets of experimental tests were performed by using the instrumented impact hammer, the first one on the direction of sensor positions, whose maximum impact force was around 19 N (see Figure 3a), and the second at the centers of the cells identified by four sensors, whose maximum impact force was around 16 N (see Figure 3b).

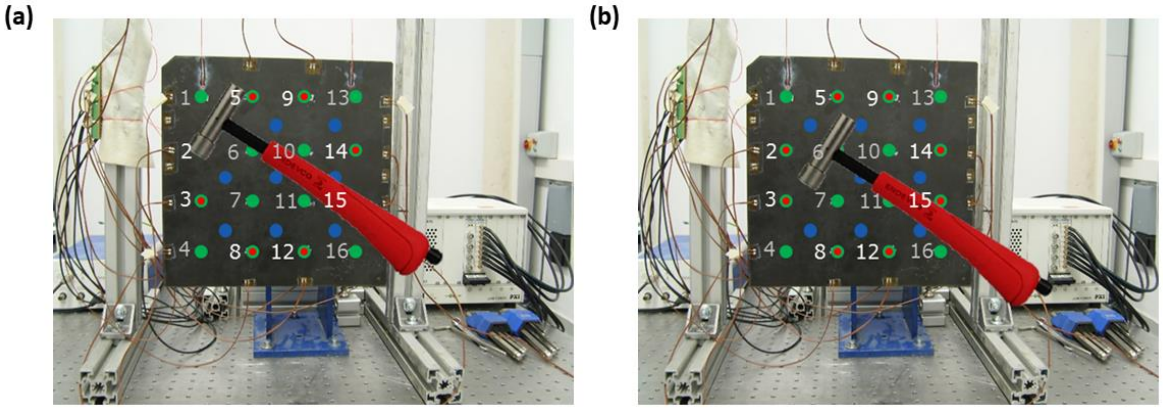

Figure 3. Experimental set-up 1 – Impact tests by instrumented hammer: impacts on the direction of sensor locations (a) and impacts between the sensors (b).

The free-drop tower consists of a steel impactor, whose weight is around 2 kg, arranged with two different heads: a 16 mm wide hemispheric head and a 35 mm cylindrical head (see Figure 4).

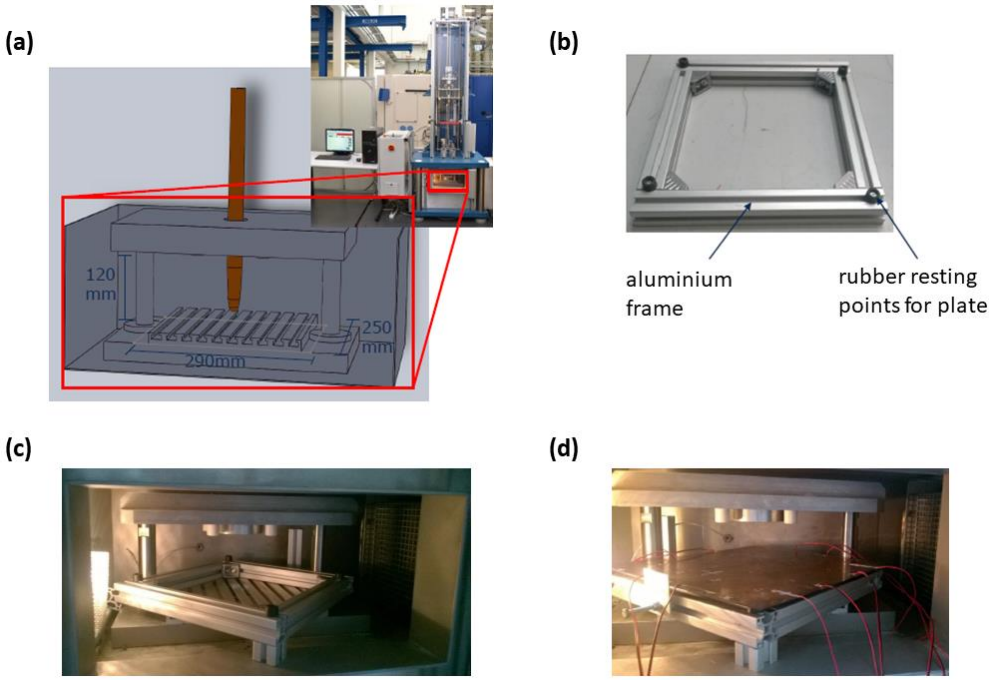

Figure 4. Experimental set-up 2 – Impact tests by free-drop tower: zoom on the testing chamber with dimensions (a); aluminum frame (b); aluminum frame in test chamber (c); aluminum frame with plate specimen in test chamber (d).

Due to limited testing area inside the testing chamber, there was just one way to place the specimen plate, and it is shown in Figure 5:

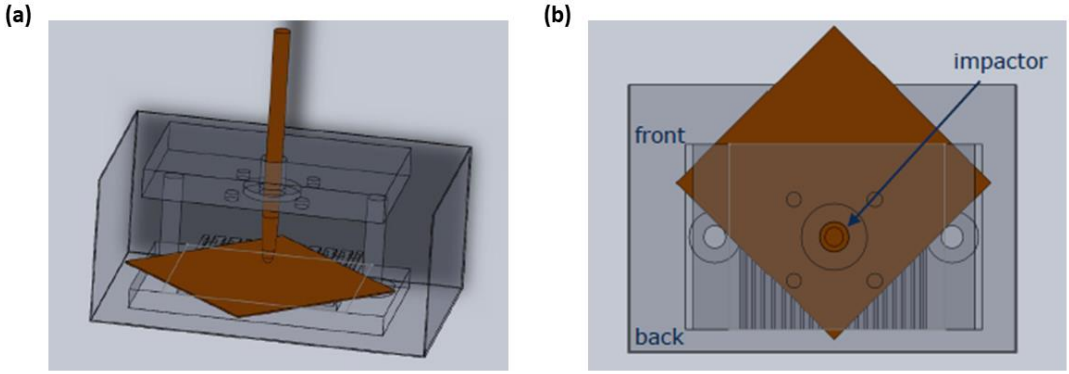

Figure 5. Test specimen located inside the testing chamber of free-drop tower: front view (a) and top view (b).

Multiple impact tests from different heights were performed at a single impact point of the specimen, all depicted in Figure 9, Figure 10 and Table 2. After each impact, an ultrasonic scan of the sample was executed (see Figure 10).

4. RESULTS

The results section is divided into two sub-sections: the first one concerns experimental tests generated by the instrumented hammer, whilst in the second one the impacts are obtained by the drop tower. In both cases, the accuracy of the impact localization algorithm is expressed by the following formula for the location error Ψ [7]:

$$\Psi = \sqrt{(x_{real} - x_{calculated})^2 + (y_{real} - y_{calculated})^2}\,, \tag{6}$$

where (x_{real}, y_{real}) are the coordinates of the true impact position and $(x_{calculated}, y_{calculated})$ are the coordinates of the calculated impact location. In all the performed experimental tests, the arbitrary set of points discussed in Sections 2.2 and 2.3 consists of 61×61 equally spaced (5 mm) points over the sample surface. For this reason, data coming from $61 \times 61 + 8$ points are considered in Eq. (5) for the calculation of impact coordinates.

4.1 Impacts generated by instrumented hammer

In Figure 6 and Figure 7, an impact between sensors 2,3,6,7 was considered. It should be noted that sensors 6 and 7 were not used in the experimental tests (see Figure 2). As exposed in Sec. 2.1, only the initial part of the recorded signals were considered for the power calculation algorithm, indeed Fig. 6b depicts some acquired signals due to the described impact event with the chosen time window. The coordinates of the true impact and the calculated one are reported in Table 1 with the location error Ψ.

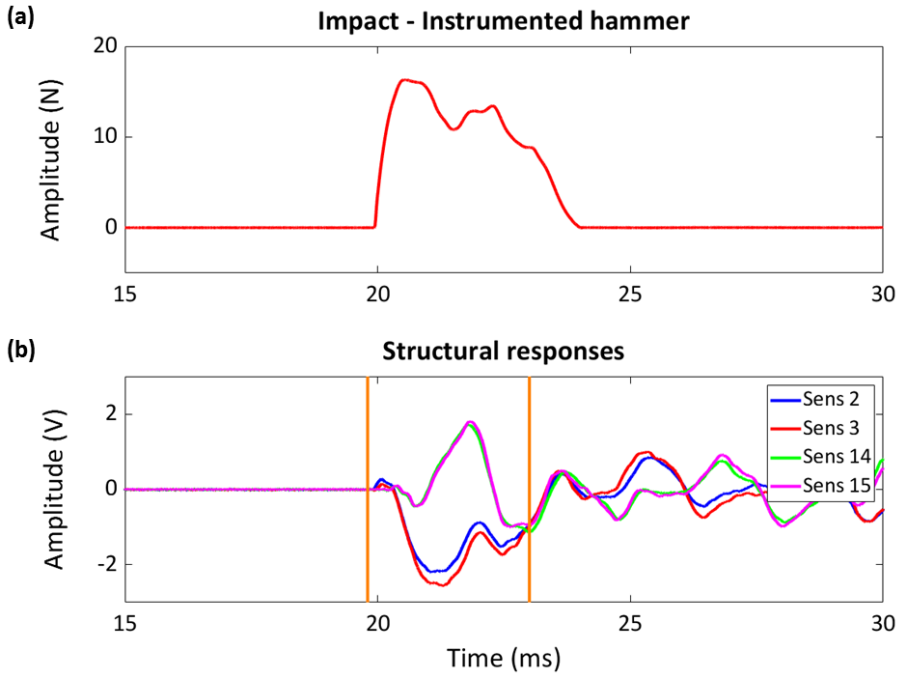

Figure 6. Impact between sensors 2,3,6,7: input signal generated by instrumented impact hammer (a) and structural responses at sensors 2,3,14,15 (b).

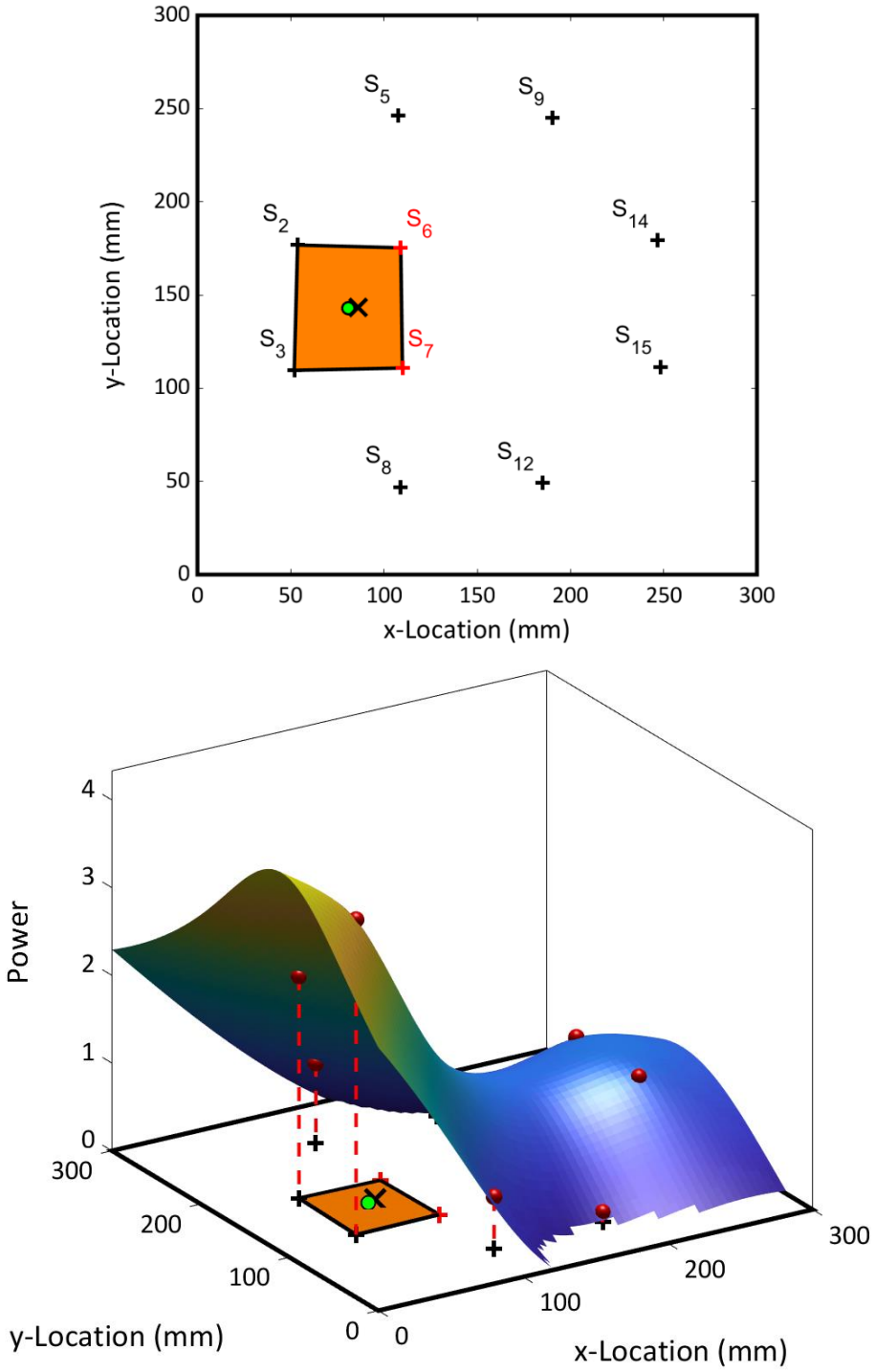

Figure 7. Impact between sensors 2,3,6,7: impact localization on a 2D plate (top) and representation of the signal power over the sample obtained by the RBF interpolation method (bottom). The real impact location is shown as a green circle, whilst the calculated one is depicted with a black cross.

Figure 8 and Table 1 show some of the results obtained by using the instrumented impact hammer. In Figure 8 the transducer locations are not reported for clarity. As reported in Table 1, the maximum location error is around 30 mm, therefore the presented method is able to localize the impact event with high accuracy. Furthermore, considering the dependency between the impact localization results and the considered time window for the recorded signals (see Section 2.1), it should be noted that the obtained results could also be improved with a different choice of time window width.

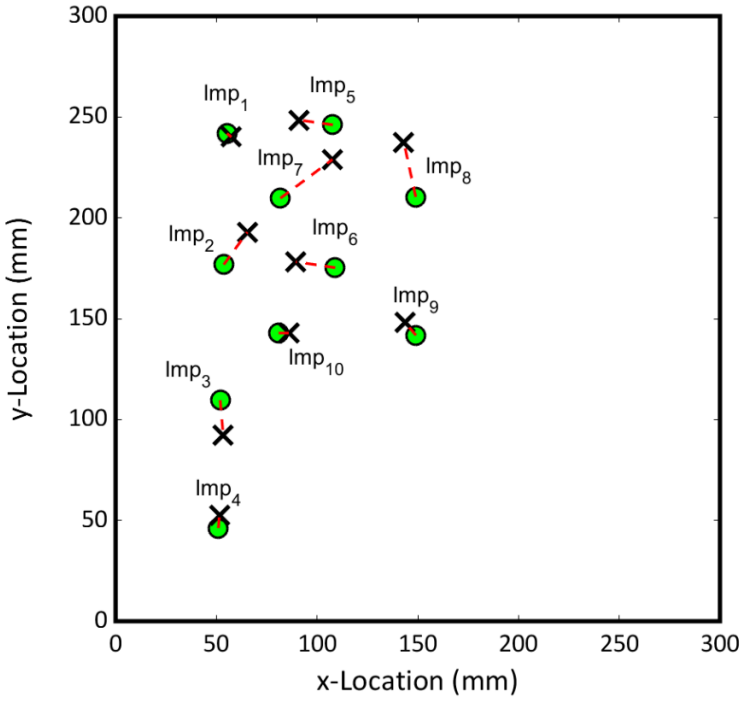

Figure 8. Experimental tests by instrumented hammer: impact localization results. The real impact locations are shown as a green circle, whilst the calculated ones are depicted with a black cross. The red dotted lines link the true impacts with the calculated ones.

Table 1. Experimental tests by instrumented hammer: impact localization results.

	x-Coord true (mm)	**y-Coord true (mm)**	**x-Coord calc (mm)**	**y-Coord calc (mm)**	**Loc err Ψ (mm)**
Impact 1	55.20	241.80	57.49	240.13	2.83
Impact 2	53.70	176.80	65.40	192.96	19.95
Impact 3	51.90	109.60	53.41	92.25	17.41
Impact 4	51	46.20	51.49	52.48	6.30
Impact 5	107.80	246.10	91.05	248.51	16.92
Impact 6	109	175.30	89.48	178.21	19.74
Impact 7	81.81	209.73	107.64	228.94	32.19
Impact 8	148.98	210.39	143.08	237.41	27.65
Impact 9	149.09	141.78	143.77	147.98	8.17
Impact 10	80.93	142.87	86.08	142.87	5.17

4.2 Impacts generated by free-drop tower

Figure 9 shows impact results related to a single impact area whose diameter was around 30 mm. Impact test details are reported in Table 2. It should be noted that location error Ψ was calculated considering the center coordinates of the impact area as the true impact location ($x_{true} = 197.2$ mm, $y_{true} = 101$ mm).

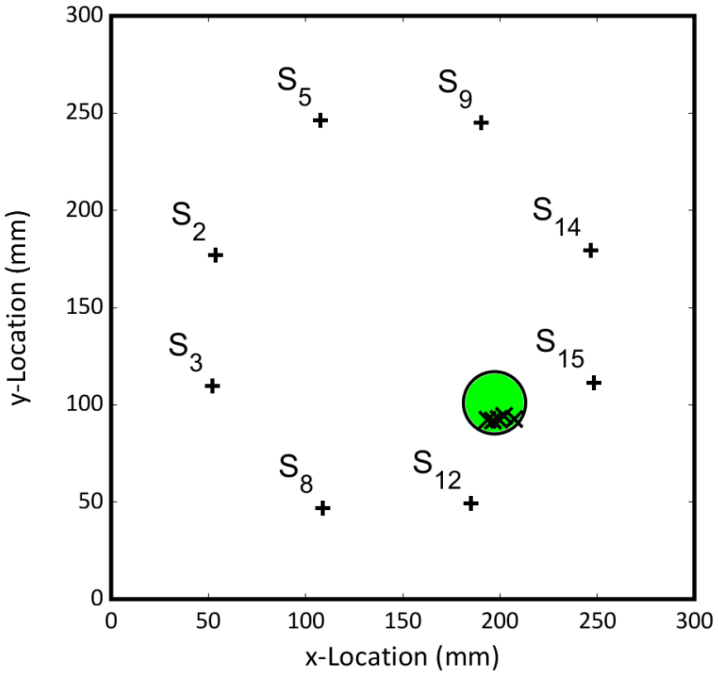

Figure 9. Experimental tests by drop tower: impact localization results. The real impact area is shown as a green circle, whilst the calculated impacts are depicted with a black cross.

Table 2. Experimental tests by drop tower: impact localization results.

	Impact Height	Impactor head	x-Coord calc (mm)	y-Coord calc (mm)	Loc err Ψ (mm)
Impact 1	400	16mm hemisphere	193.43	92.10	9.67
Impact 2	400	16mm hemisphere	199.16	92.79	8.44
Impact 3	400	16mm hemisphere	199.78	92.17	9.20
Impact 4	370	35mm cylinder	207.48	92.72	13.20
Impact 5	500	35mm cylinder	202.24	94.23	8.44
Impact 6	500	35mm cylinder	196.31	91.99	9.05

Also in the case of impact tests performed by using a drop tower, the presented results confirmed the high accuracy of the presented algorithm in the prediction of impact events. Figure 10 shows the ultrasonic scans achieved before the impact tests (reference scan) and after the Impact 6. The impact location depicted in Figure 10b coincides with the center of the impact area showed in Figure 9.

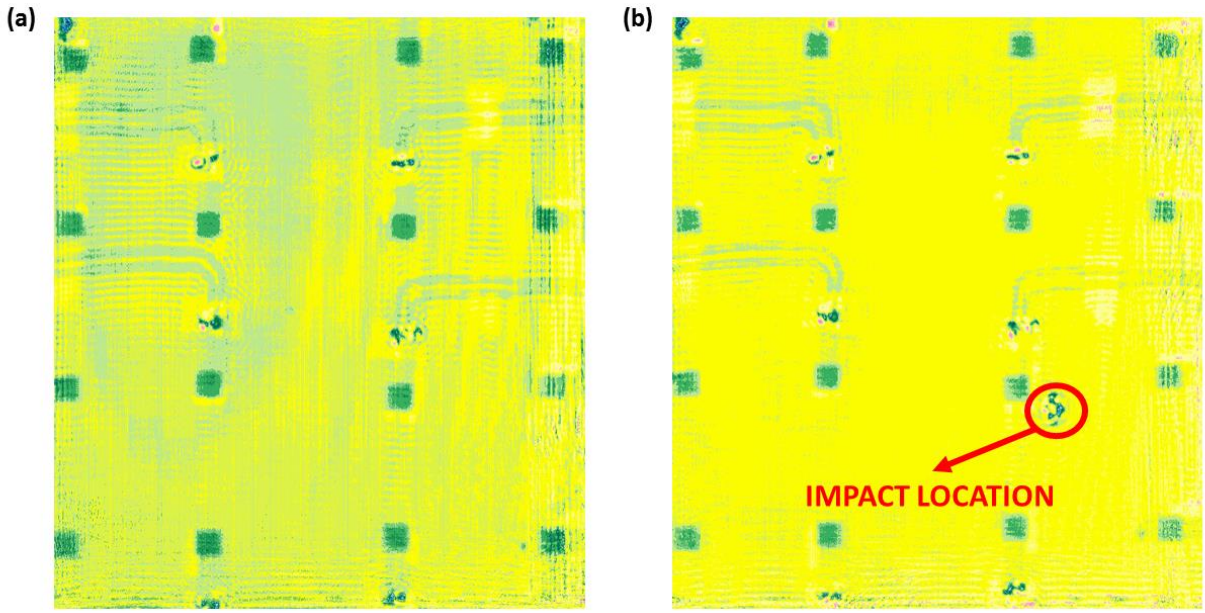

Figure 10. Ultrasonic scans: reference scan before testing (a) and scan after Impact 6 (b).

5. CONCLUSIONS

An impact localization method suitable for composite specimens arranged with a sparse array of sensors was developed and presented. The proposed algorithm is based on the power values of the first wave packets of the recorded signals due to an impact event. The calculated power values are then interpolated in an arbitrary set of points in order to obtain an improved power distribution over the entire sample. The impact coordinates are calculated by a center-of-gravity method involving all the power values and their spatial coordinates. Numerous experimental tests were performed on a CFRP plate arranged with embedded transducers, by using both an instrumented impact hammer and a small free-drop tower. The experimental test campaign confirmed the validity of the presented approach, able to estimate the coordinates of the impact event with a negligible impact location error.

ACKNOWLEDGMENTS

This paper has been funded by the EXTREME project of the European Union's Horizon 2020 research and innovation programme under grant agreement No. 636549.

REFERENCES

[1] Tobias, A., "Acoustic-emission source location in two dimensions by an array of three sensors," Non-destructive testing 9(1), 9-12 (1976).

[2] Ciampa, F. and Meo, M., "Acoustic emission source localization and velocity determination of the fundamental mode A_0 using wavelet analysis and a Newton-based optimization technique," Smart Materials and Structures 19(4), 045027.

[3] Kundu, T., Das, S. and Jata, K. V, "Point of impact prediction in isotropic and anisotropic plates from the acoustic emission data," The Journal of the Acoustical Society of America 122(4), 2057-2066 (2007).

[4] Kundu, T., Das, S., Martin, S. A. and Jata, K. V., "Locating point of impact in anisotropic fiber reinforced composite plates," Ultrasonics 48(3), 193-201 (2008).

[5] Ciampa, F. and Meo, M., "A new algorithm for acoustic emission localization and flexural group velocity determination in anisotropic structures," Composites Part A: Applied Science and Manufacturing 41(12), 1777-1786 (2010).
[6] Ciampa, F., Meo, M. and Barbieri, E., "Impact localization in composite structures of arbitrary cross section", Structural Health Monitoring, 11(6), 643-655 (2012).
[7] De Simone, M. E., Ciampa, F., Boccardi, S. and Meo, M., "Impact source localisation in aerospace composite structures", Smart Materials and Structures 26(12), 125026 (2017).
[8] Ciampa, F. and Meo, M., "Impact detection in anisotropic materials using a time reversal approach," Structural Health Monitoring 11(1), 43-49 (2012).
[9] Ciampa, F. and Meo, M., "Impact localization on a composite tail rotor blade using an inverse filtering approach," Journal of Intelligent Material Systems and Structures 25(15), 1950-1958 (2014).
[10] Ciampa, F., Boccardi S. and Meo, M., "Factors affecting the imaging of the impact location with inverse filtering and diffuse wave fields," Journal of Intelligent Material Systems and Structures 27(11), 1523-1533 (2016).
[11] De Simone, M. E., Ciampa, F. and Meo, M., "A hierarchical impact force reconstruction method for Aerospace composites," AuxDefense 2018 Conference (2018).
[12] De Simone, M. E., Ciampa, F. and Meo, M., "A hierarchical method for the impact force reconstruction in composite structures," Smart Materials and Structures (Accepted manuscript) (2018).
[13] Park, J., Ha, S. and Chang, F. K., "Monitoring impact events using a system-identification method," AIAA journal 47(9), 2011-2021 (2009).
[14] Wright, G. B., "Radial basis function interpolation: numerical and analytical developments." University of Colorado, Boulder. Doctoral dissertation (2003).
[15] Ciampa, F., Pickering, S. G., Scarselli, G. and Meo, M., "Nonlinear imaging of damage in composite structures using sparse ultrasonic sensor arrays," Structural Control and Health Monitoring 24(5), (2017).
[16] Bookstein, F. L., "Principal warps: Thin-plate splines and the decomposition of deformations," IEEE Transactions on pattern analysis and machine intelligence 11(6), 567-585 (1989).